Title

Quantitative high-efficiency cadmium-zinc-telluride SPECT with dedicated parallel-hole collimation system in obese patients: Results of a multi-center study

Journal

Journal of Nuclear Cardiology, 22(2)

ISSN

1071-3581

Authors

Nakazato, Ryo
Slomka, Piotr J
Fish, Mathews
et al.

Publication Date

2015-04-01

DOI

10.1007/s12350-014-9984-3

Peer reviewed

HHS Public Access

Author manuscript

J Nucl Cardiol. Author manuscript; available in PMC 2016 April 01.

Published in final edited form as:

J Nucl Cardiol. 2015 April ; 22(2): 266–275. doi:10.1007/s12350-014-9984-3.

Quantitative High-Efficiency Cadmium-Zinc-Telluride SPECT with Dedicated Parallel-Hole Collimation System in Obese Patients: Results of a Multi-Center Study

Ryo Nakazato, MD, PhD[1,2], **Piotr J. Slomka, PhD**[1], **Mathews Fish, MD**[3], **Ronald G. Schwartz, MD, MS**[4], **Sean W. Hayes, MD**[1], **Louise E.J. Thomson, MD**[1], **John D. Friedman, MD**[1], **Mark Lemley Jr, BS**[3], **Maria L. Mackin, CNMT, RT(N)**[4], **Benjamin Peterson, MD**[4], **Arielle M. Schwartz, BS**[4], **Jesse A. Doran, MD**[4], **Guido Germano, PhD**[1], and **Daniel S. Berman, MD**[1]

[1]Department of Imaging, Cedars-Sinai Medical Center, Los Angeles, CA

[2]Cardiovascular Center, St Luke's International Hospital, Tokyo, Japan

[3]Department of Cardiology, Peacehealth Sacred Heart Medical Center, Springfield, OR

[4]Departments of Medicine (Cardiology Division) and Imaging Sciences, University of Rochester Medical Center, Rochester, NY

Abstract

Background—Obesity is a common source of artifact on conventional SPECT myocardial perfusion imaging (MPI). We evaluated image quality and diagnostic performance of high-efficiency (HE) cadmium-zinc-telluride (CZT) parallel-hole SPECT-MPI for coronary artery disease (CAD) in obese patients.

Methods and Results—118 consecutive obese patients at 3 centers (BMI 43.6±8.9 kg/m^2, range 35–79.7 kg/m^2) had upright/supine HE-SPECT and ICA >6 months (n=67) or low-likelihood of CAD (n=51). Stress quantitative total perfusion deficit (TPD) for upright (U-TPD), supine (S-TPD) and combined acquisitions (C-TPD) was assessed. Image quality (IQ; 5=excellent; <3 nondiagnostic) was compared among BMI 35–39.9 (n=58), 40–44.9 (n=24) and ≥45 (n=36) groups. ROC-curve area for CAD detection (≥50% stenosis) for U-TPD, S-TPD, and C-TPD were 0.80, 0.80, and 0.87, respectively. Sensitivity/specificity was 82%/57% for U-TPD, 74%/71% for S-TPD, and 80%/82% for C-TPD. C-TPD had highest specificity (*P*=.02). C-TPD normalcy rate was higher than U-TPD (88% vs. 75%, *P*=.02). Mean IQ was similar among BMI 35–39.9, 40–44.9 and ≥45 groups [4.6 vs. 4.4 vs. 4.5, respectively (*P*=.6)]. No patient had a non-diagnostic stress scan.

Address for Correspondence: Daniel S. Berman, MD, Department of Imaging, Cedars-Sinai Medical Center, 8700 Beverly Boulevard, Taper Building Suite 1258, Los Angeles, CA 90048, USA, Phone: 310-423-4223, Fax: 310-423-0811, bermand@cshs.org.

Conflicts of interest:

Dr. Piotr Slomka, Guido Germano and Dr. Daniel Berman receive royalties from the software employed in the study. Dr. Mathews Fish is a medical consultant of Spectrum-Dynamics. Dr. Daniel Berman is a shareholder in Spectrum-Dynamics. All others disclose no conflict of interest.

Conclusions—In obese patients, HE-SPECT MPI with dedicated parallel-hole collimation demonstrated high image quality, normalcy rate, and diagnostic accuracy for CAD by quantitative analysis of combined upright/supine acquisitions.

Keywords

myocardial perfusion imaging; obesity; cadmium-zinc-telluride; parallel-hole collimation; quantification

INTRODUCTION

Obesity is associated with an increased risk of cardiovascular disease and cardiac mortality (1), and its prevalence has increased markedly over the past several decades. In 2009–2010, over 78 million adults in the United States were obese, estimated to be 35% of the adult population. Obesity is a source of artifact in all forms of cardiac imaging. On single-photon emission computed tomography (SPECT) myocardial perfusion imaging (MPI), excess soft tissue attenuation of radioactivity frequently produces artifactual myocardial perfusion defects (2, 3).

Recently, two new high-efficiency SPECT (HE-SPECT) cameras with cadmium-zinc-telluride (CZT) semiconductor detectors have been introduced (4) and have been validated by coronary angiography for the detection of coronary artery disease (CAD) (5–7). Some data are available regarding detection of coronary artery disease (CAD) in obese patients using a multi-pinhole collimation system with CZT detectors (8, 9). However, no study to date has evaluated the use of a CZT SPECT system with dedicated parallel-hole collimation in obese patients. Thus, the aim of this study was to evaluate image quality and diagnostic performance of HE-SPECT with dedicated parallel-hole collimation system in obese patients for detection of CAD.

MATERIALS AND METHODS

Study Patients

The total study population consisted of 118 consecutive obese patients [defined as body mass index (BMI) ≥35 kg/m^2] with suspected CAD who underwent clinically indicated rest/stress HE-SPECT MPI performed in both upright and supine position at 3 centers (Cedars-Sinai Medical Center, Peacehealth Sacred Heart Medical Center, University of Rochester Medical Center) between 2008 and 2013. The mean BMI was 43.6 ± 8.9 kg/m^2 and maximum BMI was 79.7 kg/m^2. The patients were stratified by degree of obesity categorized as BMI 35–39.9 kg/m^2 (n = 58), 40–44.9 kg/m^2 (n = 24) and ≥45 kg/m^2 (n = 36) groups, with the latter two groups defined as morbidly obese (BMI ≥40 kg/m^2) (10). The research use of clinical and imaging data for this study was IRB approved by each institution.

Angiographic Validation Cohort—For comparison of HE-SPECT vs. invasive coronary angiography (ICA), we studied 67 consecutive obese patients [mean BMI 41.0 ± 6.2 kg/m^2, maximum 68.1 kg/m^2] who had ICA within 6 months after HE-SPECT and having none of

the following: (a) prior myocardial infarction or coronary revascularization; (b) nonischemic cardiomyopathy or valvular heart disease; and (c) change in symptoms between SPECT and ICA. Patient characteristics are listed in the Table 1. Mean age was 58 ± 11 years and mean BMI was 41.0 ± 6.2 kg/m^2 (maximum 68.1 kg/m^2). Exercise stress was employed in 16 (24%) patients, all of whom achieved the maximal target heart rate during exercise. Average time between HE-SPECT and ICA was 22 ± 28 days.

Image Quality and Normalcy Rate Assessment Cohort—Image quality was assessed in the angiographic validation cohort as well as in 51 consecutive obese patients [mean BMI 46.9 ± 10.7 kg/m^2, maximum 79.7 kg/m^2, mean age 52 ± 12] who had a low likelihood of CAD (<10%) based on age, sex, symptoms, coronary risk factor and results of treadmill stress test at the time of HE-SPECT (5). The majority of the low likelihood patients were asymptomatic patients undergoing assessment before bariatric surgery. Most of the remaining patients were assessed asymptomatic patients referred prior to other surgical procedures.

Stress and Acquisition Protocols

A rest/stress ^{99m}Tc-sestamibi protocol was utilized in 111 patients. A stress ^{201}Tl/rest ^{99m}Tc-sestamibi protocol was utilized in 7 patients due to shortage of ^{99m}Tc. The details of stress and image acquisition protocols have been previously described (5, 11, 12). Average injected dose was 400 ± 215 MBq (10.8 ± 5.8 mCi) for rest and 1350 ± 252 MBq (36.5 ± 6.8 mCi) for stress in the rest/stress ^{99m}Tc-sestamibi protocol, and 104 ± 22 MBq (2.8 ± 0.6 mCi) for stress and 359 ± 56 MBq (9.7 ± 1.5 mCi) for rest in the stress ^{201}Tl/rest ^{99m}Tc-sestamibi protocol. Length of the acquisition time was varied depending on the injected dose.

Rest/stress ^{99m}Tc-sestamibi Protocol—A 6–12 min rest image acquisition was performed in the upright position beginning 30 to 60 min after injection, followed by a 6–12 min supine acquisition in patients tested during the latter period of the study. Patients then underwent standard exercise treadmill testing or pharmacological stress. Beginning 15 to 30 min after stress injection, 2–6 min stress image acquisitions were performed in the upright and supine positions.

Stress ^{201}Tl/rest ^{99m}Tc-sestamibi Protocol—After exercise stress or pharmacological stress, a 6-min supine stress acquisition was performed followed by a 6-min upright acquisition. Subsequently, without moving the patient from the imaging chair, ^{99m}Tc-sestamibi was injected and a 4-min rest upright acquisition was performed followed by a 4-min supine rest acquisition. In four patients, we used an acquisition protocol based on left ventricular counts, in which the time of acquisition is adjusted to achieve 1,000,000 left ventricular counts (13).

HE-SPECT Scanner and Imaging Method

A full description of the system performance of the HE-SPECT system used in this study (D-SPECT, Spectrum-Dynamics, Haifa, Israel) has been previously reported (14–16). The system uses 9 tungsten collimated CZT detector columns rotating in synchrony, each

consisting of 1024 (16 × 64), 5-mm thick CZT elements (2.46 × 2.46 mm). The size of the collimator holes matches the dimensions of the detector elements. Before imaging, the detector was positioned parallel to the patient's chest, with the heart in the center of the field of view. A 10-sec pre-scan acquisition was performed to identify the location of the heart and to set the angle limits of scanning for each detector column (region-of-interest centric scanning). Each image set was acquired with 120 projections per detector. Transaxial images were generated from list mode data by the use of a proprietary reconstruction algorithm based on the maximum likelihood expectation maximization method (16). No attenuation or scatter correction was applied, instead 2-position imaging was used as described above to recognize attenuation artifacts. Images were then reoriented into short-axis and vertical and horizontal long-axis slices using standard software (QPS, Cedars-Sinai Medical Center, Los Angeles, California).

Automated Quantification of HE-SPECT MPI

All image datasets were transferred to Cedars-Sinai Medical Center and were analyzed by a single experienced core laboratory technologist without knowledge of clinical data. Automatically generated myocardial contours by QPS software were evaluated and when necessary, contours were adjusted to correspond to the myocardium. We used a separate normal database for each radiopharmaceutical (5). We used both upright and supine images for quantitative analysis in this study. Upright and supine images were quantified separately using their respective upright and supine normal perfusion limits (5). The quantitative perfusion variable employed, total perfusion deficit (TPD), is a combination of both defect severity and the extent of the defect (17). Stress perfusion defects on HE-SPECT were assessed by quantification of the TPD (5, 18). In addition to deriving separate TPD measures for upright TPD (U-TPD) and supine TPD (S-TPD), we applied a combined quantification approach and obtained combined upright/supine TPD (C-TPD) values, as previously described (5). In brief, C-TPD was calculated by limiting the TPD computation from the supine polar map to pixels which have been quantified as abnormal on upright images (mean absolute deviation >3.0). The same threshold (mean absolute deviation >3.0) was used for supine images, but only in locations determined to be abnormal on upright images; locations quantified as normal by upright imaging were not considered. Therefore, C-TPD represents the magnitude of perfusion defect seen on both supine and upright images in the same location. C-TPD parameter was expressed in the same units (percentage of the myocardium) as in the separate supine and upright TPD measures. The thresholds of U-TPD ≥5%, S-TPD ≥5%, and C-TPD ≥3% were considered abnormal, as previously established (5).

Visual Scoring of HE-SPECT MPI

Visual semi-quantitative scoring was performed by experienced imaging cardiologists during routine clinical reading using a 17-segment, 5-point scoring system (0 = normal, 1 = equivocal, 2 = moderate, 3 = severe reduction of radioisotope uptake, and 4 = absence of detectable tracer uptake) (19), with the reader being aware of all imaging data (upright and supine static and ECG-gated images), patient history, and stress test results. Visual semi-quantitative scoring was performed using both upright and supine images. Separate scoring of upright and supine images was not performed. Summed stress scores were obtained by adding the scores of the 17-segments and expressed as percentage of abnormal myocardium

at stress (SSS%myo) by dividing the summed maximum score 68 (4 × 17) and multiplying by 100 as previously described (20). SSS%myo ≥5% was considered abnormal (21).

Assessment of Image Quality

HE-SPECT images of the 118 patients were assessed for overall image quality at separate times and in random order by 2 readers. Each reader scored overall image quality on a 5 point scale (5 = excellent, 4 = good, 3 = fair, 2= poor, 1 = uninterpretable) as well as for the amount of extra-cardiac activity on a 5 point scale (0 = none; 1 = minimal and without any interference with scan interpretability; 2 = mild and probably without any interference with interpretability; 3 = moderate and probably interfering with scan interpretability; 4 = severe and definitely interfering with scan interpretability). Discrepancy between readers was addressed by subsequently reviewing the images jointly and assigning a consensus classification. Average values of upright and supine images are reported for image quality and extra-cardiac activity. Image quality <3 was considered nondiagnostic. Different categories of image quality are illustrated in Figure 1.

ICA Analysis

All ICA studies were interpreted visually by experienced cardiologists who were unaware of clinical information of the HE-SPECT results. Patients did not have myocardial infarction or revascularization in the interval between HE-SPECT and ICA. A ≥50% luminal diameter stenosis by visual assessment was considered obstructive.

Statistical Analysis

Statistical analyses were performed with SPSS 19.0 (www.SPSS.com, Chicago, IL). All continuous variables were described as mean ± SD and categorical variables are presented as frequencies. For 3 group comparisons, a one-way ANOVA test with Scheffe correction for multiple pair-wise comparisons was used for continuous variables, and Pearson Chi-square test or Fisher exact test was used as appropriate for categorical variables. Receiver-operating-characteristic (ROC) curve analysis was performed in angiographic validation cohort to evaluate the ability of the quantification to predict ≥50% stenosis of coronary arteries. ROC curves were created using a step of 0.1% for the TPD and SSS%myo values, then the differences between ROC curve areas (area ± SE) were compared. Sensitivity and specificity between different types of acquisition were compared using a paired McNemar's test. In terms of the individual coronary territories, sensitivity and specificity were calculated at a cutoff point disease severity of 50% luminal diameter narrowing on ICA. A two-tailed $p < 0.05$ was considered statistically significant.

RESULTS

Obstructive CAD was found in 39 of the 67 patients who had ICA. Single, double, or triple vessel or left main stenoses were present in 20, 7, and 12, respectively. Regarding the distribution of stenoses, the numbers of patients with left main, left anterior descending artery, left circumflex and right coronary artery lesions were 4, 25, 12 and 23, respectively.

TPD from Upright, Supine and Combined Quantitative Analysis and Visual Analysis

Of the 67 patients who underwent HE-SPECT and ICA, 44 patients had perfusion defects with U-TPD ≥5 % on upright alone, 37 had defects with S-TPD ≥5 % on supine alone, 36 had defects with C-TPD ≥3 % on combined analysis, and 39 had defects with SSS%myo ≥5 % on visual analysis. TPD (mean ± SD) are follows in 0–1 and 2–3 vessel disease groups. [0–1 vessel disease]; U-TPD = 6.9 ± 6.7, S-TPD = 6.1 ± 6.4, C-TPD = 3.6 ± 5.8. [2–3 vessel disease]; U-TPD = 15.5 ± 8.5, S-TPD = 13.8 ± 8.3, C-TPD = 12.7 ± 8.9. Examples of combined upright-supine stress MIBI images in two morbidly obese patients are shown in Figures 2 and 3.

Diagnostic Performance of HE-SPECT

ROC curves for the detection of CAD by TPD measures derived from upright, supine, combined upright-supine datasets and visual assessment are shown in Figure 4. The areas under the ROC curves for U-TPD, S-TPD, C-TPD and SSS%myo were 0.80 [95% confidence interval (CI) 0.69–0.91], 0.80 (0.69–0.91), 0.87 (0.78–0.95), and 0.84 (0.75–0.93), respectively. C-TPD had highest area under the ROC curve and showed trend toward significance compared to U-TPD ($P = 0.06$) or S-TPD ($P = 0.07$).

Sensitivity/specificity for detection of ≥50% stenosis were 82%/57% for U-TPD, 74%/71% for S-TPD, 80%/82% for C-TPD and 82%/75% for SSS%myo (Figure 5). Accuracy was 72% (95% CI 59–82%) for U-TPD, 73% (61–83%) for S-TPD, 81% (69–89%) for C-TPD and 79% (67–88%) for SSS%myo. For the quantitative analysis, the sensitivity was relatively similar among U-TPD, S-TPD and C-TPD and ($P = NS$). However, the specificity was significantly improved in C-TPD when compared to U-TPD ($P < .01$).

Normalcy rates for U-TPD, S-TPD and C-TPD and SSS were 75%, 78%, 88%, and 100% respectively. C-TPD yielded a significantly higher normalcy rate when compared with U-TPD in low likelihood patients (88% vs. 75%, $P = .02$).

Image Quality of HE-SPECT

Image quality (IQ) by BMI is summarized in Table 2. Mean IQ was similar among BMI 35–39.9, 40–44.9 and ≥45 kg/m^2 groups [4.6 vs. 4.4 vs. 4.5 for stress ($P = .6$), 4.4 vs. 4.4 vs. 4.3 for rest ($P = .8$)] (Table 2). No patients had a non-diagnostic stress scan; three patients had non-diagnostic rest scan. There was no significant difference in extra-cardiac activity among 3 obese groups for stress [0.3 vs. 0.3 vs. 0.3 for stress ($P = .8$)] (Table 3).

DISCUSSION

This is the first multi-center study that has investigated the diagnostic performance and image quality of quantitative HE-CZT SPECT with the dedicated parallel-hole collimation system in obese patients for detection of CAD compared with ICA. We observed with the combined upright–supine approach, the sensitivity for detection of CAD by TPD assessment was 80%, the specificity for the absence of CAD was 82%, and the normalcy rate was 88%. Image quality with this parallel-hole CZT SPECT system was high in this population of consecutively selected obese patients, including 60 patients in the morbidly obese group

(BMI ≥40 kg/m^2) of whom 36 had BMI ≥45 kg/m^2. Remarkably, none of the patients had a nondiagnostic stress SPECT study.

Previously, using a CZT camera with multi-pinhole collimation (Alcyone; GE Healthcare), Fiechter et al. reported poor diagnostic quality in morbidly obese patients (8). Image quality was reportedly nondiagnostic in 81% and was marginally decreased to 55% by the use of CT-based attenuation correction in this important population. They concluded the poor quality was likely due to the difficulty in positioning such obese patients in the limited field-of-view of this multi-pinhole collimation system. In contrast, the parallel-hole collimation system used in our study is relatively easily positioned, even in the severely obese patients (up to 79.7 kg/m^2 in this study). Further, the system uses a proprietary "ROI-centric" imaging that allows the center of imaging to be placed over the heart, even in severely obese patients in whom the heart is positioned far from the surface of the chest wall.

As with all other SPECT systems that do not employ attenuation correction, the HE-SPECT images can be affected by soft-tissue artifacts; however, these artifacts are mitigated by the use of the routine two position image acquisitions. We have previously shown that detection of CAD is more accurate with combined upright and supine HE-SPECT MPI than with upright imaging alone in general population (5). In the current study, we found favorable diagnostic performance in a consecutive series of obese patients using combined upright and supine HE-CZT SPECT MPI. Visual read (SSS%myo) and C-TPD provided comparable accuracy. It should be noted, however, that the interpreters were highly experienced in D-SPECT interpretation. The specificity and the normalcy rates were significantly higher when analysis of both upright and supine images as assessed by C-TPD was employed. Similarly, visual read improve the specificity over U-TPD. The slightly lower normalcy rate of 88% in this study compared to prior SPECT-MPI literature may in part be due to the higher pre-test risk of this referred "low likelihood" population in the current era of the routine use of appropriate use criteria (22).

It is generally recommended that a two day SPECT protocol be in morbidly obese patients when using traditional Anger cameras. The several fold higher sensitivity afforded by the HE-CZT SPECT camera permits routine clinical imaging of this morbidly obese population with a one day protocol.

We used quantitative analysis for the interpretation of the HE-SPECT studies as well as visual assessment. Quantitative analysis eliminates observer variability and bias and has been shown to be useful in comparing sequential SPECT MPI studies (23, 24) and assessing the effectiveness of invasive and medical treatments in patients with CAD (18). Quantitative analysis also provides an approach that might be more generalizable to other centers not dependent on the expertise of the interpreter for analysis with the new gamma-camera.

LIMITATIONS

Our study has several limitations. It was a retrospective analysis of patients who had undergone HE-SPECT for clinical purposes. In the group subsequently undergoing ICA, this practice results in a selection bias, as patients with abnormal SPECT findings are more likely to be referred for ICA. Different acquisition protocols were applied in the current

study over time, and our current protocol which appears to optimize study quality and accuracy by obtaining one million counts in the left ventricle region of interest was used in only 4 cases in the current study. Semi-quantitative visual analysis was only performed using the combination of upright and supine static and gated images during routine clinical reading; separate visual analysis of results in upright, supine, and combined images was not performed. We recognize anatomic ≥50% luminal diameter stenosis, which we used in the present study, may not be an optimal standard for functional stenosis severity. Fractional flow reserve, which might have provided a better comparator for hemodynamically significant stenosis, was not performed in most of the patients in this study. Additionally, the sensitivity and specificity for angiographic CAD observed in this study could have been affected by referral bias as well as by the small number of patients with angiographic CAD.

NEW KNOWLEDGE GAINED

In this first multi-center study in obese patients using HE-CZT SPECT with a dedicated parallel-hole collimation system, we found high image quality and high diagnostic accuracy for the detection of CAD on ICA.

CONCLUSIONS

In this multicenter study of obese patients, including 60 morbidly obese patients, HE-SPECT with a dedicated parallel-hole collimation system had high image quality and high diagnostic accuracy for detection of CAD by both quantitative and visual analyses. The combination of upright and supine acquisitions appears to improve the specificity for the detection of CAD in obese patients. Based on this multicenter experience, HE-SPECT with parallel-hole collimation using upright and supine imaging appears to be an accurate and reliable method for evaluation of CAD in the important, increasingly prevalent and diagnostically challenged obese population.

Acknowledgments

This research was partially supported in part by Grant R01-HL089765 from the National Heart, Lung, and Blood Institute/National Institutes of Health (NHLBI/NIH).

Abbreviations List

SPECT	single-photon emission computed tomography
MPI	myocardial perfusion imaging
HE-SPECT	high-efficiency SPECT
CZT	cadmium-zinc-telluride
CAD	coronary artery disease
BMI	body mass index
ICA	invasive coronary angiography
TPD	total perfusion deficit

U-TPD	upright TPD
S-TPD	supine TPD
C-TPD	combined upright/supine TPD
SSS%myo	percentage of abnormal myocardium at stress
ROC	receiver-operating-characteristic
IQ	image quality

References

1. Jensen MD, Ryan DH, Apovian CM, Loria CM, Ard JD, Millen BE, et al. 2013 AHA/ACC/TOS Guideline for the Management of Overweight and Obesity in Adults: A Report of the American College of Cardiology/American Heart Association Task Force on Practice Guidelines and The Obesity Society. J Am Coll Cardiol. 2013
2. DePuey EG. How to detect and avoid myocardial perfusion SPECT artifacts. J Nucl Med. 1994; 35:699–702. [PubMed: 8151397]
3. DePuey EG, Garcia EV. Optimal specificity of thallium-201 SPECT through recognition of imaging artifacts. J Nucl Med. 1989; 30:441–9. [PubMed: 2661749]
4. Slomka P, Patton J, Berman D, Germano G. Advances in technical aspects of myocardial perfusion SPECT imaging. J Nucl Cardiol. 2009; 16:255–76. [PubMed: 19242769]
5. Nakazato R, Tamarappoo BK, Kang X, Wolak A, Kite F, Hayes SW, et al. Quantitative upright-supine high-speed SPECT myocardial perfusion imaging for detection of coronary artery disease: correlation with invasive coronary angiography. J Nucl Med. 2010; 51:1724–31. [PubMed: 20956478]
6. Duvall WL, Sweeny JM, Croft LB, Barghash MH, Kulkarni NK, Guma KA, et al. Comparison of high efficiency CZT SPECT MPI to coronary angiography. J Nucl Cardiol. 2011; 18:595–604. [PubMed: 21638154]
7. Gimelli A, Bottai M, Genovesi D, Giorgetti A, Di Martino F, Marzullo P. High diagnostic accuracy of low-dose gated-SPECT with solid-state ultrafast detectors: preliminary clinical results. Eur J Nucl Med Mol Imaging. 2012; 39:83–90. [PubMed: 21887532]
8. Fiechter M, Gebhard C, Fuchs TA, Ghadri JR, Stehli J, Kazakauskaite E, et al. Cadmium-zinc-telluride myocardial perfusion imaging in obese patients. J Nucl Med. 2012; 53:1401–6. [PubMed: 22870823]
9. Gimelli A, Bottai M, Giorgetti A, Genovesi D, Filidei E, Marzullo P. Evaluation of ischaemia in obese patients: feasibility and accuracy of a low-dose protocol with a cadmium-zinc telluride camera. Eur J Nucl Med Mol Imaging. 2012; 39:1254–61. [PubMed: 22699527]
10. Sturm R. Increases in morbid obesity in the USA: 2000–2005. Public Health. 2007; 121:492–6. [PubMed: 17399752]
11. Sharir T, Slomka P, Hayes S, DiCarli M, Ziffer J, Martin W, et al. Multicenter trial of high-speed versus conventional single-photon emission computed tomography imaging: quantitative results of myocardial perfusion and left ventricular function. J Am Coll Cardiol. 2010; 55:1965–74. [PubMed: 20430269]
12. Berman D, Kang X, Tamarappoo B, Wolak A, Hayes S, Nakazato R, et al. Stress thallium-201/rest technetium-99m sequential dual isotope high-speed myocardial perfusion imaging. JACC Cardiovasc Imaging. 2009; 2:273–82. [PubMed: 19356571]
13. Nakazato R, Berman DS, Hayes SW, Fish M, Padgett R, Xu Y, et al. Myocardial perfusion imaging with a solid-state camera: simulation of a very low dose imaging protocol. J Nucl Med. 2013; 54:373–9. [PubMed: 23321457]
14. Patton J, Slomka P, Germano G, Berman D. Recent technologic advances in nuclear cardiology. J Nucl Cardiol. 2007; 14:501–13. [PubMed: 17679058]

15. Sharir T, Ben-Haim S, Merzon K, Prochorov V, Dickman D, Berman D. High-speed myocardial perfusion imaging initial clinical comparison with conventional dual detector anger camera imaging. JACC Cardiovasc Imaging. 2008; 1:156–63. [PubMed: 19356422]
16. Gambhir S, Berman D, Ziffer J, Nagler M, Sandler M, Patton J, et al. A novel high-sensitivity rapid-acquisition single-photon cardiac imaging camera. J Nucl Med. 2009; 50:635–43. [PubMed: 19339672]
17. Slomka PJ, Nishina H, Berman DS, Akincioglu C, Abidov A, Friedman JD, et al. Automated quantification of myocardial perfusion SPECT using simplified normal limits. J Nucl Cardiol. 2005; 12:66–77. [PubMed: 15682367]
18. Shaw LJ, Berman DS, Maron DJ, Mancini GB, Hayes SW, Hartigan PM, et al. Optimal medical therapy with or without percutaneous coronary intervention to reduce ischemic burden: results from the Clinical Outcomes Utilizing Revascularization and Aggressive Drug Evaluation (COURAGE) trial nuclear substudy. Circulation. 2008; 117:1283–91. [PubMed: 18268144]
19. Berman D, Kiat H, Friedman J, Wang F, van Train K, Matzer L, et al. Separate acquisition rest thallium-201/stress technetium-99m sestamibi dual-isotope myocardial perfusion single-photon emission computed tomography: a clinical validation study. J Am Coll Cardiol. 1993; 22:1455–64. [PubMed: 8227805]
20. Hachamovitch R, Hayes S, Friedman J, Cohen I, Berman D. Comparison of the short-term survival benefit associated with revascularization compared with medical therapy in patients with no prior coronary artery disease undergoing stress myocardial perfusion single photon emission computed tomography. Circulation. 2003; 107:2900–7. [PubMed: 12771008]
21. Nakazato R, Berman DS, Gransar H, Hyun M, Miranda-Peats R, Kite FC, et al. Prognostic value of quantitative high-speed myocardial perfusion imaging. J Nucl Cardiol. 2012; 19:1113–23. [PubMed: 23065414]
22. Hendel R, Berman D, Di Carli M, Heidenreich P, Henkin R, Pellikka P, et al. ACCF/ASNC/ACR/AHA/ASE/SCCT/SCMR/SNM 2009 Appropriate Use Criteria for Cardiac Radionuclide Imaging: A Report of the American College of Cardiology Foundation Appropriate Use Criteria Task Force, the American Society of Nuclear Cardiology, the American College of Radiology, the American Heart Association, the American Society of Echocardiography, the Society of Cardiovascular Computed Tomography, the Society for Cardiovascular Magnetic Resonance, and the Society of Nuclear Medicine. J Am Coll Cardiol. 2009; 53:2201–29. [PubMed: 19497454]
23. Berman D, Kang X, Gransar H, Gerlach J, Friedman J, Hayes S, et al. Quantitative assessment of myocardial perfusion abnormality on SPECT myocardial perfusion imaging is more reproducible than expert visual analysis. J Nucl Cardiol. 2009; 16:45–53. [PubMed: 19152128]
24. Slomka P, Berman D, Germano G. Quantification of serial changes in myocardial perfusion. J Nucl Med. 2004; 45:1978–80. [PubMed: 15585470]

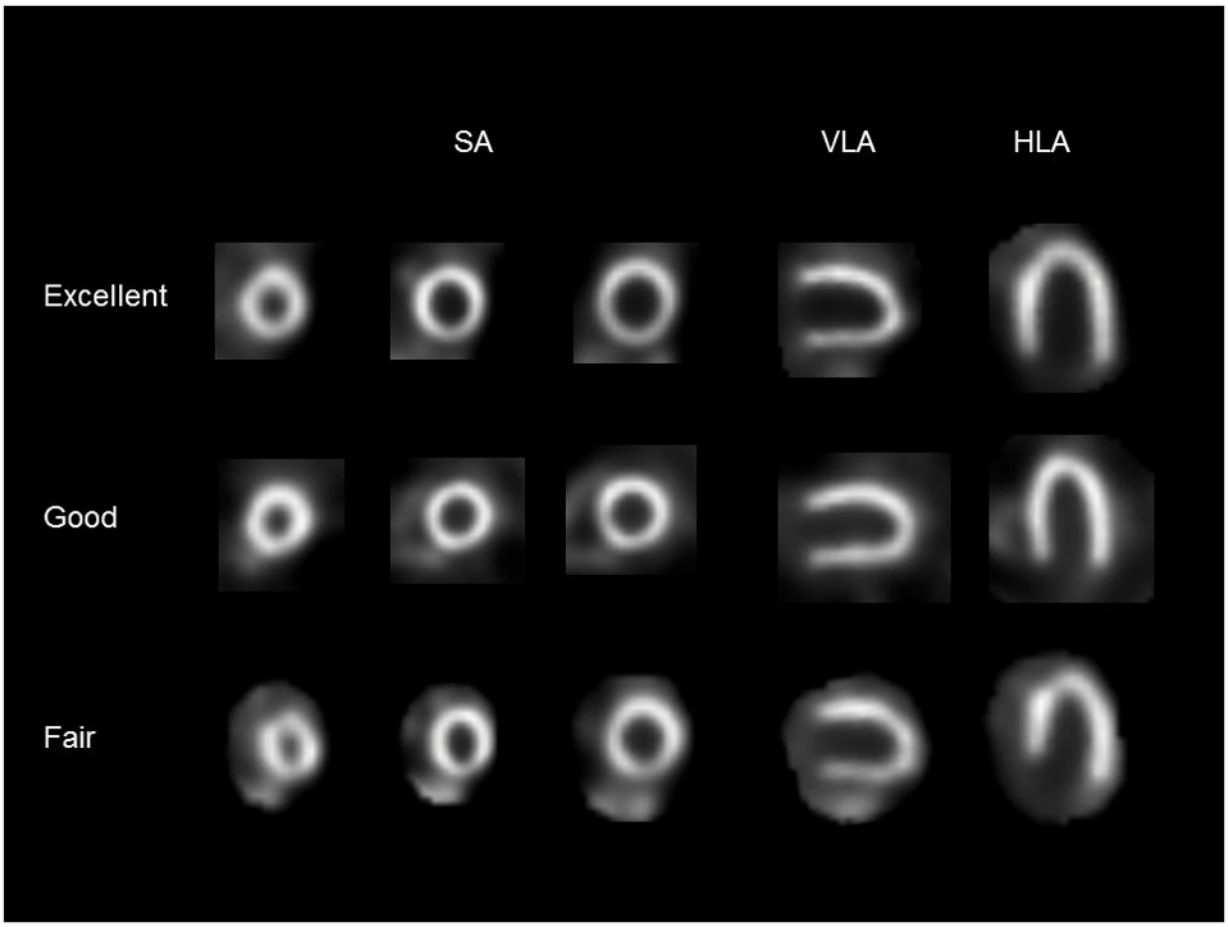

Figure 1.
Case examples of different cactegories of image quality are displayed in 3 short axis (SA), vertical long axis (VLA), and horizontal long axis (HLA). A: Excellent, B: Good, C: Fair.

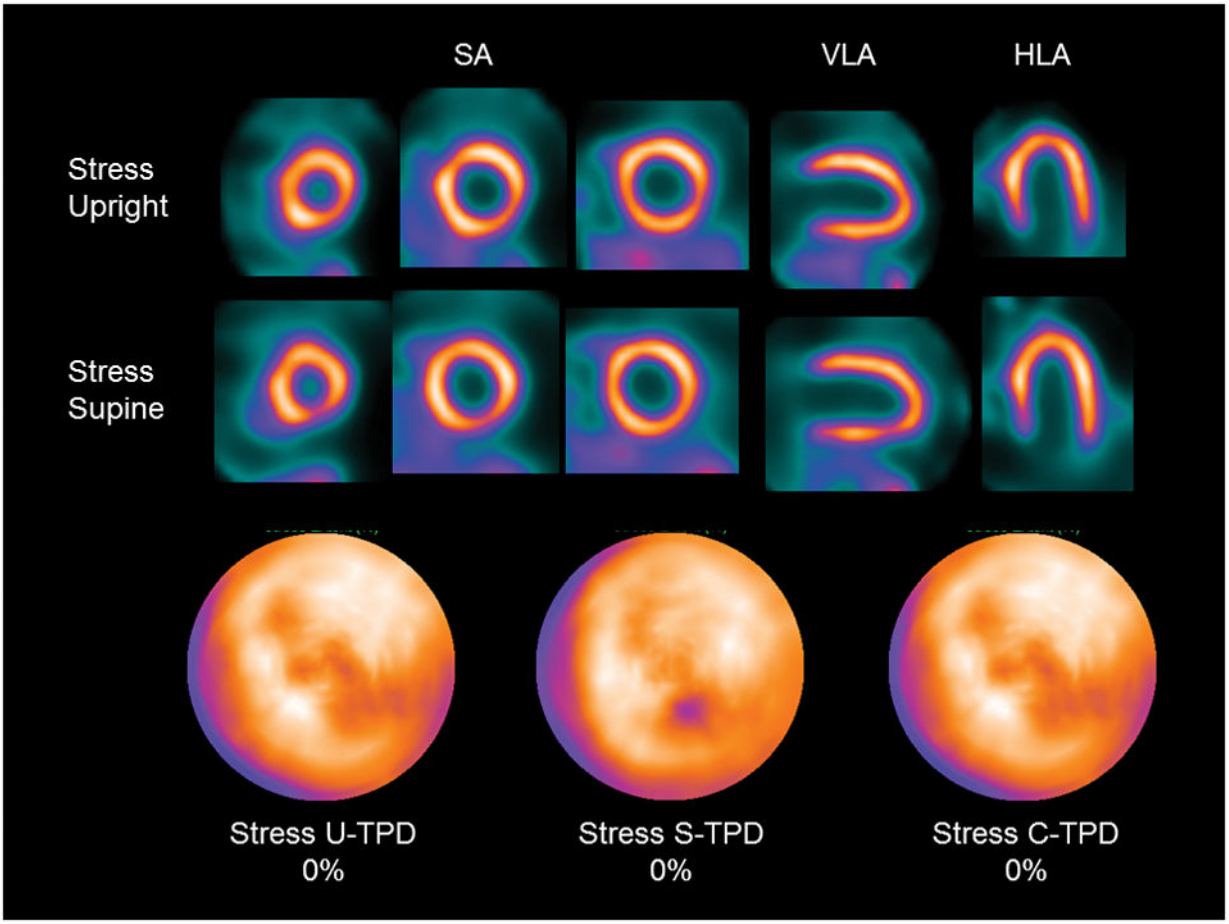

Figure 2.

Example of stress HE-SPECT images in a 48 year old morbidly obese male patient (BMI 60.2 kg/m^2) and no stenosis on coronary angiography. Images are displayed in 3 short axis (SA), vertical long axis (VLA), and horizontal long axis (HLA). Upright and supine images show no reduced uptake of radiotracer (top and middle row). Blackout maps are shown (bottom row) and quantification results were 0% for U-TPD and 0% for S-TPD. When upright and supine images are combined, no defect is visualized on black-out map, with C-TPD of 0% (bottom row).

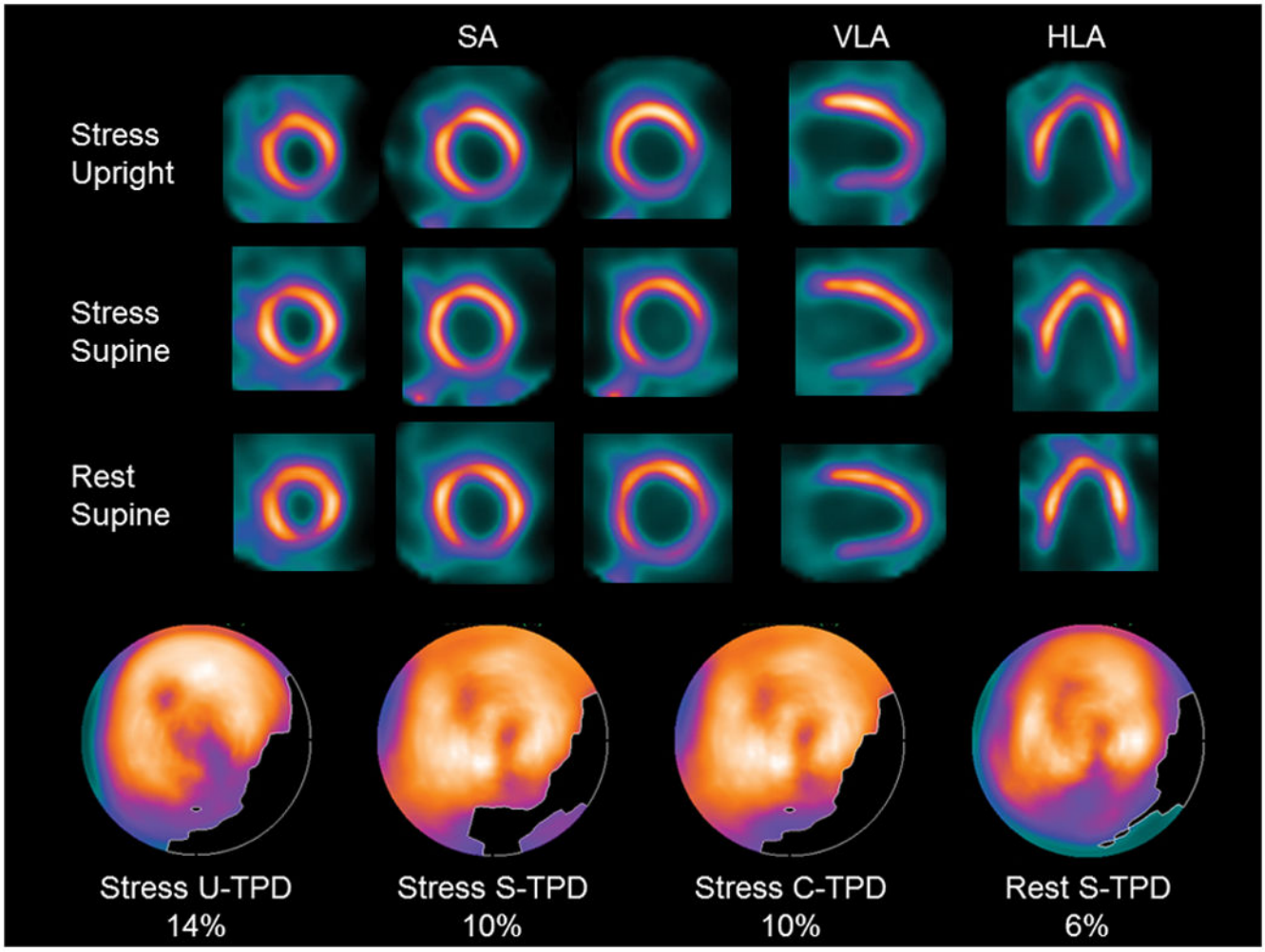

Figure 3.

Example of stress and rest HE-SPECT images in a 67 year old morbidly obese male patient (BMI 42.6 kg/m^2) with severe stenosis of the proximal right coronary artery and an occluded left circumflex artery on coronary angiography. Both upright (top row) and supine (middle row) stress images show apparent inferolateral wall perfusion abnormality, and rest supine image show lateral wall perfusion abnormality. Stress U-TPD, S-TPD, C-TPD and rest S-TPD are 14%, 10%, 10% and 6%, respectively. Black-out maps (bottom row) illustrate the corresponding perfusion defects.

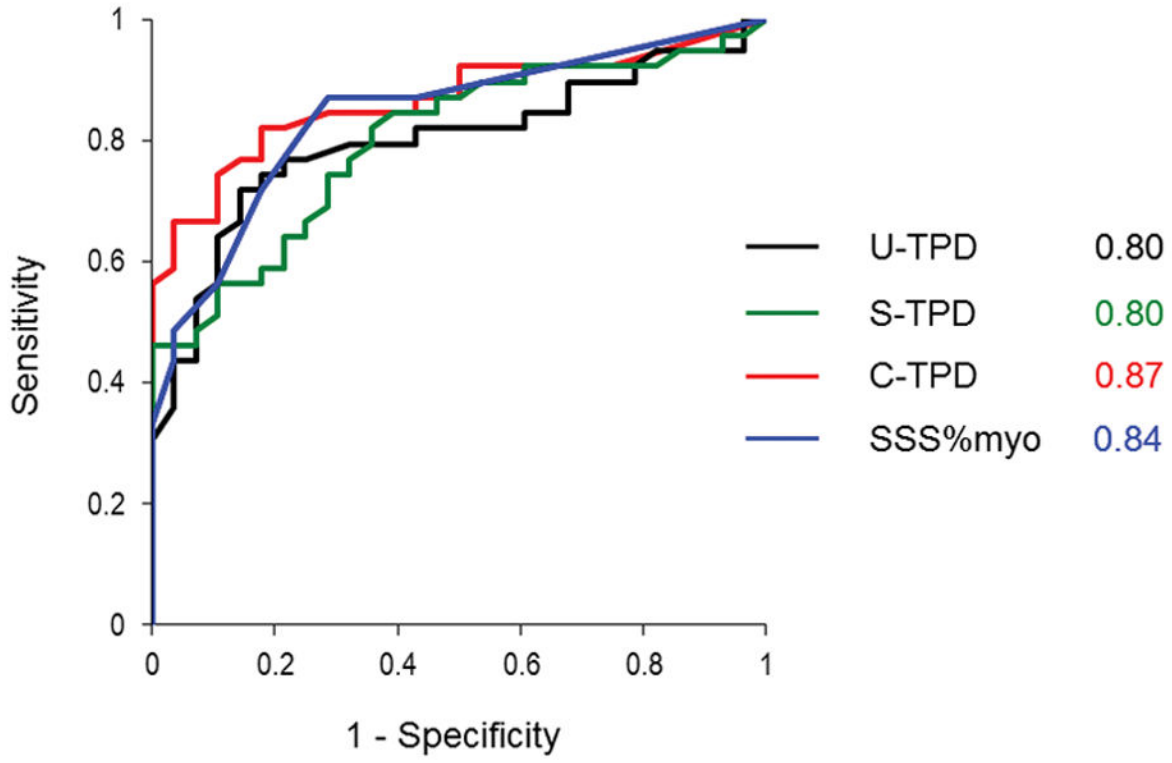

Figure 4.

ROC curves for detection of CAD by measurements of U-TPD, S-TPD, C-TPD and SSS %myo. Percentage TPD was compared with presence or absence of CAD as observed by ICA. C-TPD had highest area under the ROC curve (*P* = NS against U-TPD and S-TPD).

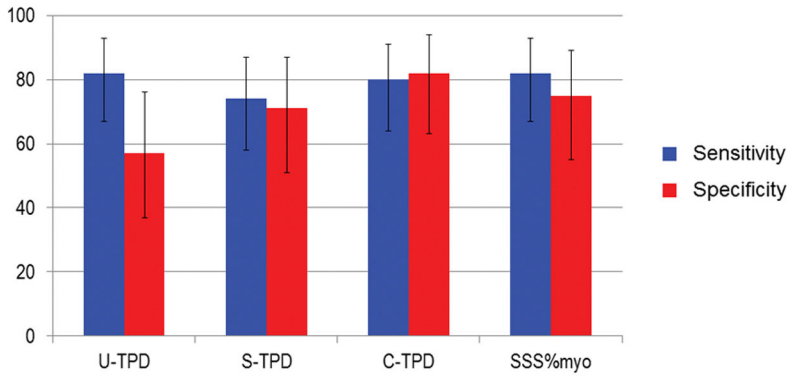

Figure 5.

Diagnostic performance of quantitative and visual analysis. Sensitivities and specificities for detection of CAD by U-TPD, S-TPD, C-TPD and SSS%myo (bars depicted the 95% CI). Specificity was significantly improved in C-TPD when compared to U-TPD ($P < .01$).

Table 1

Baseline Variables

	Total n = 118	**Angiographic cohort n = 67**
Age	55 ± 12	58 ± 11
Men	58 (49%)	34 (51%)
BMI (kg/m^2)	43.6 ± 8.9	41.0 ± 6.2
BMI 35–39.9, n	58	38
BMI 40–44.9, n	24	19
BMI ≥45, n	36	10
Hypertension	87 (73%)	54 (81%)
Diabetes	35 (30%)	35 (52%)
Dyslipidemia	60 (51%)	43 (64%)
Smoking	25 (21%)	13 (19%)
Typical angina	9 (8%)	9 (13%)
Atypical angina	19 (16%)	19 (28%)
Shortness of breath	17 (14%)	17 (25%)
Asymptomatic	57 (48%)	7 (10%)
Exercise stress	25 (21%)	12 (18%)

BMI, Body mass index

Table 2

Image quality

Stress	**BMI 35–39.9 (n = 58)**	**BMI 40–44.9 (n = 24)**	**BMI ≥45 (n = 36)**	***P* value**	**Overall (n = 118)**
Excellent	44	15	27	-	-
Good	11	6	6	-	-
Fair	3	3	3	-	-
Poor	0	0	0	-	-
Uninterpretable	0	0	0	-	-
Mean score ± SD	4.6 ± 0.6	4.4 ± 0.7	4.5 ± 0.7	.6	4.6 ± 0.7

Rest	**BMI 35–39.9 (n = 58)**	**BMI 40–44.9 (n = 24)**	**BMI ≥45 (n = 36)**	***P* value**	**Overall (n = 118)**
Excellent	35	16	20	-	-
Good	15	5	13	-	-
Fair	6	3	2	-	-
Poor	2	0	1	-	-
Uninterpretable	0	0	0	-	-
Mean score ± SD	4.4 ± 0.8	4.4 ± 0.7	4.3 ± 0.8	.8	4.4 ± 0.8

Table 3

Extra-cardiac activity

Stress	**BMI 35–39.9 (n = 58)**	**BMI 40–44.9 (n = 24)**	**BMI ≥45 (n = 36)**	***P* value**	**Overall (n = 118)**
None	48	17	30	-	-
Minimal	8	7	6	-	-
Mild	2	0	0	-	-
Moderate	0	0	0	-	-
Severe	0	0	0	-	-
Mean score ± SD	0.3 ± 0.5	0.3 ± 0.5	0.3 ± 0.4	.8	0.3 ± 0.5

Rest	**BMI 35–39.9 (n = 58)**	**BMI 40–44.9 (n = 24)**	**BMI ≥45 (n = 36)**	***P* value**	**Overall (n = 118)**
None	29	11	28	-	-
Minimal	25	11	8	-	-
Mild	4	2	0	-	-
Moderate	0	0	0	-	-
Severe	0	0	0	-	-
Mean score ± SD	0.7 ± 0.6	0.8 ± 0.6	0.4 ± 0.4	.02	0.6 ± 0.6